**Boise State University**
## ScholarWorks

10-14-2018

# Carbon-Coated FeP Nanoparticles Anchored on Carbon Nanotube Networks as Anode for Long-Life Sodium-Ion Storage

Chunrong Ma
*Shanghai Jiao Tong University*

Zhengguang Fu
*Chinese Academy of Sciences*

Changjian Deng
*Boise State University*

XiaoZhen Liao
*Shanghai Jiao Tong University*

YuShi He
*Shanghai Jiao Tong University*

**See next page for additional authors**

**Authors**

Chunrong Ma, Zhengguang Fu, Changjian Deng, XiaoZhen Liao, YuShi He, ZiFeng Ma, and Hui Xiong

ROYAL SOCIETY OF CHEMISTRY

# ChemComm

## COMMUNICATION

# Carbon-Coated FeP Nanoparticles Anchored on Carbon Nanotube Networks as Anode for Long-Life Sodium-Ion Storage

Chunrong Ma,[a] Zhengguang Fu,[b] Changjian Deng,[c] XiaoZhen Liao,[a] YuShi He,[a] ZiFeng Ma, *[a,d] and Hui Xiong *[c]

**A novel electrode design strategy of carbon-coated FeP particles anchored on a conducting carbon nanotube network (CNT@FeP-C) is designed to achieve a superior sodium ion storage. Such a unique structure demonstrated excellent long-life cycling stability (a 95% capacity retention for more than 1200 cycles at 3 A g$^{-1}$) and rate capability (delivered 272 mAh g$^{-1}$ at 8 A g$^{-1}$).**

In the past decades, lithium-ion batteries (LIBs) have attracted extensive attention in electric vehicles and portable electronic devices[1-4]. However, the surging cost and limited resources of lithium have restricted its application for large-scale energy storage systems coupled with intermittent renewable power generation[5]. In contrast, sodium-ion batteries (SIBs) as an attractive alternative to LIBs have obtained renewed attention because of the natural abundance and low cost of sodium raw materials. Nevertheless, great challenges still remain in realizing SIB's full potentials. The sluggish kinetics and severe volume changes during Na$^+$ insertion/extraction caused by the larger sodium ion (1.02 Å) lead to poor cycling stability and rate capability, which present significant challenges for future SIB advancements[6-10]. Therefore, it is critically important to develop electrode materials with enhanced Na$^+$ storage and transport properties as well as structural stability to overcome these issues.

Iron phosphide (FeP) has attracted increased intention in recent years due to its good electrochemical activity for hydrogen evolution reaction[11, 12], but the application of FeP in SIBs is still in the early stage. Wang et al.[13] reported that a graphene wrapped FeP anode exhibited an initial discharge capacity of about 1000 mAh g$^{-1}$ at 0.1 A g$^{-1}$ but only retained ~400 mAh g$^{-1}$ after 250 cycles. Li et al.[12] prepared CoP/FeP composite electrode interconnected by reduced graphene oxide, which displayed 480 mAh g$^{-1}$ at a current density of 100 mA g$^{-1}$. Nevertheless, the long-term cycling performance in the reported FeP anode materials is not satisfactory especially at fast charge/discharge rates due to their intrinsically low electronic conductivity and the large volume change during sodiation/desodiation process. Hence, in order to improve the electrochemical properties of FeP-based anodes, an effective approach is to combine the merits of the electrically and ionically conducting carbon and FeP utilizing a unique nanostructure.

Herein, we demonstrate an anode based on carbon-coated FeP nanoparticles anchored on carbon nanotube networks (CNT@FeP-C), which could keep the FeP nanoparticles within flexible carbon hosts and maintain monodispersity among the hosts concurrently. This strategy has several advantages: (1) the interconnected conductive network from CNTs and carbon shell at the nanoparticles favor fast electron/ion transfer and transport, promoting superior rate capability; (2) the CNT networks as backbones are crucial to maintain monodispersity of active materials and thus can decrease the stress from particle agglomeration; (3) the elastic carbon shell can relieve the mechanical stress resulted from the volume expansion/contraction during Na$^+$ insertion/extraction processes and protect the active particles from corrosion. When evaluated as the anode for SIBs, the CNT@FeP-C composite electrode exhibited ultra-long cycling performance and superior rate capability.

X-ray diffraction (XRD) was used to study the crystal structure and phase of the CNT@ FeP-C (Figure S1a, Supporting Information). The diffraction pattern of this material is in good agreement with the orthorhombic FeP (JCPDS no. 65-2595). The XRD result suggests that the material is free of impurities. It also suggests that the materials have a small grain size, which is calculated to be ~ 2 nm according to the Scherrer equation[14]. The Raman spectrum in Figure S1b exhibits two distinct peaks centered at ~1356 and ~1600 cm$^{-1}$, corresponding to the D band for disorder sp$^2$ carbon, and the G band for in

a. *Shanghai Electrochemical Energy Devices Research Centre, School of Chemistry and Chemical Engineering, Shanghai Jiao Tong University, Shanghai, 200240, China.*

b. *Qingdao Institute of Bioenergy and Bioprocess Technology, Chinese Academy of Sciences, Qingdao, 266101, China.*

c. *Micron School of Materials Science and Engineering, Boise State University, Boise, ID 83725, USA. E-mail: clairexiong@boisestate.edu*

d. *Sinopoly Battery Research Centre, Shanghai, 200241, China.*
† Footnotes relating to the title and/or authors should appear here.

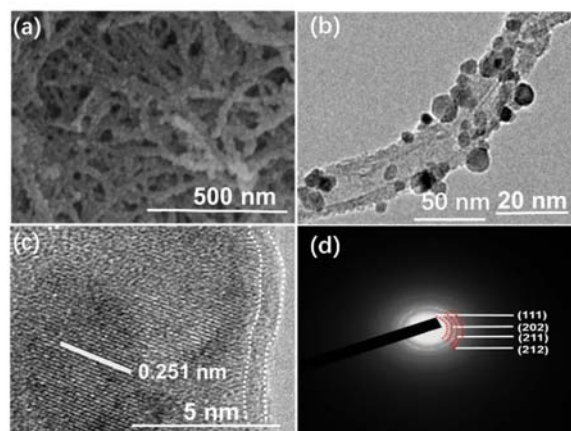**ARTICLE**                                                                                      Journal Name



**Figure 1**. (a) SEM image, (b-d) TEM images and selected area electron diffraction of the CNT@FeP-C.



**Figure 2.** (a) XPS survey spectrum, (b−d) High-resolution XPS spectrum of Fe 2p, P 2p, and C 1s of CNT@FeP-C.

plane vibration of graphitic $sp^2$ carbons. The integrated intensity ratio ($I_D/I_G$) is about 0.8, indicating the presence of highly crystallized carbon[15], which favors fast electron transfer. Compared to FeP ($10^{-2}$ S m$^{-1}$), CNT@FeP-C exhibits a remarkable increase in electrical conductivity by up to 2 order of magnitude (8 S m$^{-1}$), promoting the electron transport for enhanced electrochemical reactions. Furthermore, the actual content of the FeP in the as-prepared sample was evaluated by thermogravimetric analysis (TGA). From Figure S2 (Supporting Information), a small weight loss occurs at below 200 ℃, which can be explained by the removal of surface water, while the second weight loss between 200 to 300 ℃ is ascribed to the amorphous carbon coating (5%)[13]. Finally, the distinct weight loss from 300 to 600 ℃ is attributed to the combined effects of the oxidation of FeP[13] and decomposition of CNT. According to the TGA results of FeP and CNT@FeP-C, the weight content of FeP and carbon in the composite is calculated to be about 59.3% and 36.7%, respectively.

The structure and morphology of the as-prepared sample were investigated by the scanning electron microscopy (SEM) and transmission electron microscopy (TEM). Compared with pure CNT shown in Figure S3 (Supporting Information), the CNT@FeP-C preserves the one-dimensional nanostructure of the CNT with diameters ranging from 20 to 24 nm (Figure 1a). The surface of CNT becomes coarse in the composite, indicating a successful coating of FeP nanoparticles with carbon. Monodispersed FeP nanoparticles can be clearly observed in Figure 1b, FeP particles with sizes between 4 and 8 nm are homogeneously anchored on the CNT surface. The HRTEM image (Figure 1c) shows that the FeP nanoparticle is wrapped by an amorphous carbon layer. Meanwhile, the lattice fringes with a 0.251 nm *d*-spacing corresponding to the (102) plane of FeP are shown in Figure 1d, which is in good agreement with the XRD result. Four bright diffraction rings can be identified in the selected-area electron diffraction (SAED) pattern (Figure 2d), which correspond to the (111), (202), (211) and (212) planes of the orthorhombic FeP (JCPDS no. 65-2595). The diffraction rings indicate that material is nanocrystalline. The carbon layer introduced during the first hydrothermal process demonstrated a
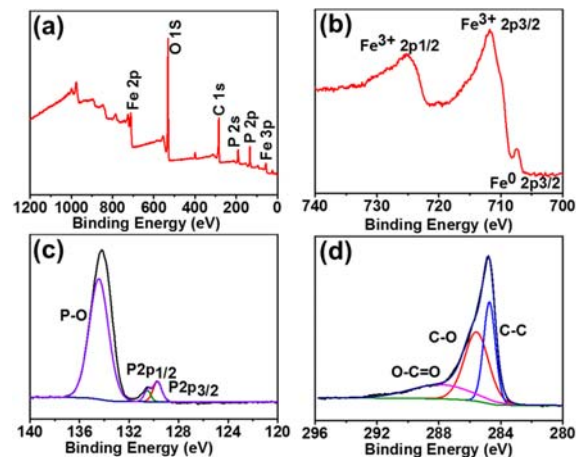
significant role such that it preserves the monodispersity of FeP nanoparticles, and suppresses the growth of primary nanoparticles during the hydrothermal and annealing process at the same time.

XPS was used to study the surface element electronic state and chemical components of the CNT@FeP-C nanocomposite. The survey spectrum demonstrates the existence of Fe, P, C and O elements at the sample surface (Figure 2a). The high resolution XPS Fe 2p spectrum (Figure 2b) shows peaks with binding energy centered at 707.7 and 720.9 eV, corresponding to the Fe (II) 2p$_{3/2}$ and 2p$_{1/2}$ peaks, respectively. The peaks centered at 713.3 and 727.2 eV can be explained by the oxidized Fe species in FeP due to prolonged exposure to air[11]. For P 2p high resolution spectrum (Figure 2c), there are two main peaks: P 2p$_{3/2}$ and P 2p$_{1/2}$ at 129.3 and 130.1 eV, respectively, which are characteristic of FeP. Meanwhile, the high binding energy peak located at 133.6 eV could be assigned to the P species associated with the oxidation of the sample during the measurement[11]. As for the high resolution C 1s spectrum (Figure 2d), it can be deconvoluted into four peaks: the main peak located at 284.4 eV ascribed to C=C/C-C and the three peaks at 285.4, 286.5 and 288.7 eV corresponding to C≡C/C-C, C=O and O-C=O, respectively. $N_2$ adsorption-desorption isotherm is shown in Figure S4 (Supporting Information) with a typical IV isotherm. The specific Brunauer-Emmett-Teller (BET) area of the CNT@FeP-C is 138.4 m$^2$ g$^{-1}$.

The discharge-charge profile of the electrode in the voltage range of 0.01~ 3 V at 500 mA g$^{-1}$ is illustrated in Figure 3a. The CNT@FeP-C electrode delivers a discharge capacity of 700 mAh g$^{-1}$ and charge capacity of 425 mAh g$^{-1}$ with an initial Coulombic efficiency (CE) of 60.7%. The large initial capacity loss is attributed to the formation of irreversible $Na_2O$ and a SEI layer[13]. In the following cycles, the discharge and charge curves almost overlap and the corresponding CE value is as high as 99%. The rate performance of the CNT@FeP-C nanocompvsiete is shown in Figure 3b. The anode delivers a stable discharge
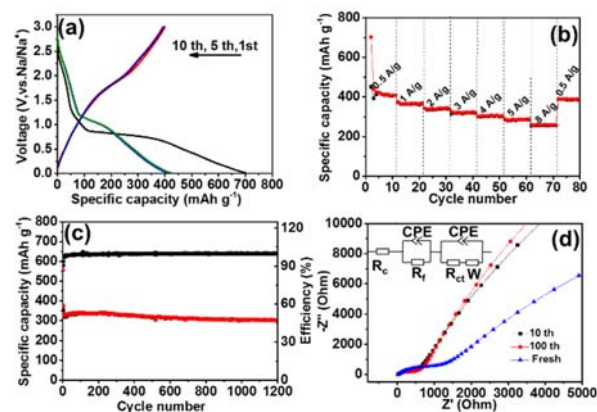
**Figure 3**. Electrochemical performance of the CNT@FeP-C. (a) The charge-discharge profiles, (b) The rate capability of the CNT@FeP-C, (c) The long-term cycling performance of the CNT@FeP-C electrode at the current rate of 3 A g$^{-1}$, and (d) Nyquist plots of the electrodes (Inset: equivalent circuit model used for fitting).

capacity of 264 and 340 mAh g$^{-1}$ at high current density of 1 and 2 A g$^{-1}$, respectively. Furthermore, when the current density is increased to 5 A g$^{-1}$, a high reversible capacity of 285 mAh g$^{-1}$ is maintained during subsequent cycles. As the rate is set back to 500 mA g$^{-1}$, the capacity could be recovered to 386 mAh g$^{-1}$ and remains stable in the following cycles. It is worth noting that the rate study was performed after 5 initial cycles at a low rate, which was used to fully activate the electrode. The long-term cycling performance of the CNT@FeP-C nanocomposite electrode was evaluated at a current density of 3 A g$^{-1}$ (Figure 3c). The CNT@FeP-C nanocomposite electrode maintains a reversible capacity of 321 mAh g$^{-1}$ after 1200 cycles without noticeable decay, which indicates that the electrode exhibits a superior long-term cycling stability.

The cycling performance of FeP and CNT control samples were also conducted to compare with the CNT@FeP-C nanocomposite electrode. As shown in Figure S5 (Supporting Information), the FeP and CNT electrodes only deliver 165 and 30 mAh g$^{-1}$ after 100 cycles at 1 A g$^{-1}$, respectively, which are significantly inferior to the performance of the CNT@FeP-C. Considering of the poor performance of pure FeP and CNT electrodes, it strongly suggests that CNT only contributes a small portion in the whole sodium ion storage of CNT@FeP-C but it can play a critical role in keeping the mono<u>dispersity</u> of the nanoparticle, maintaining structure stability and enhancing electrical and ion conductivity. To investigate the electrochemical properties of the CNT@FeP-C nanocomposite electrode, electrochemical impedance spectroscopy (EIS) measurements were conducted. The Nyquist plots (Figure 3d) are characterized by a depressed semicircle in the high-to-medium frequency range and a straight sloping line in the low frequency region. The kinetic parameters can be determined by fitting the measured impedance spectra with an equivalent circuit model (Figure 3d). $R_e$ and $R_f$ are the ohmic resistance and the SEI film resistance, respectively. $R_{ct}$ represent the charge-transfer resistance at the electrode surface. $Z_w$ is the Warburg impedance, which can be associated with the diffusion of sodium ions into the active electrode. It is found that the R$_e$ stays almost the same

among all samples, $Z_w$ increased gradually from 103.4 to 126.1 and 129.2 Ω after 10 and 100 cycles. The increase of $Z_w$ from the first cycle to subsequent cycles can be explained by the inevitable formation of SEI film[14]. In addition, the $R_{ct}$ values decreased after the initial cycle and remained fairly stable after 100 cycles (385 and 392 Ω after 10 and 100 cycles, respectively), revealing an improved charge transfer kinetics. Moreover, the diffusion coefficient of Na$^+$ within the active materials can be calculated according to the following equation[16] :

$$D_{Na^+} = \frac{R^2 T^2}{2A^2 n^4 F^4 C^2 \sigma^2}\qquad(1)$$

where $A$ is the surface area of electrode, $n$ is the number of electron transfer, $F$ is the Faraday constant, $C$ is the molar concentration of Na$^+$, and $\sigma$ is the Warburg factor calculated from the slope of the lines between Z' and ω$^{-1/2}$ (the inset in Figure S6) through equation (2):

$$Z' = R_D + R_L + \sigma\omega^{-1/2}\qquad(2)$$

The $D_{Na^+}$ values of the electrode before cycling and after 10 and 100 cycles are 5.64×10$^{-13}$ cm$^2$ s$^{-1}$, 3.12×10$^{-12}$ cm$^2$ s$^{-1}$, 3.68×10$^{-12}$ cm$^2$ s$^{-1}$, respectively. It is apparent that the Na$^+$ diffusivity in the electrode is enhanced after cycling and remains stable with further cycling. Comparing to other metal phosphide electrode[17, 18], the CNT@FeP-C electrode showed higher $D$ value, revealing faster Na$^+$ diffusion kinetics. This is possibly due to the high structural integrity of CNT@FeP-C, which can help explain its superb rate capability as shown earlier in this section.

The sodium ion storage property of CNT@FeP-C was investigated by cyclic voltammetry (CV) (Figure 4a). The initial cathodic process is dramatically different from the subsequent cycles, two distinct peaks can be observed at ~0.75 and 0.29 V vs. Na/Na$^+$, which could be explained by the sodiation process and the formation of SEI film on the electrode, respectively[19]. In the following cycles, the peak at ~ 0.29 V disappears, indicating the irreversible formation of SEI and that the formed SEI is stable. The anodic peak centered around 1.85 V almost overlap in all cycles, which can be attributed to Na$^+$ removal from the Na$_x$FeP phase, showing an outstanding reversible Na$^+$ extraction[20]. The sodiation of FeP could be described as follows[13, 19, 20]:

$$Fep + xNa^+ \rightarrow Na_x FeP\qquad(3)$$
$$Na_x FeP + (3-x)Na^+ + (3-x)e^- \rightarrow Na_3 P + Fe\quad(4)$$
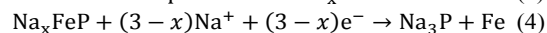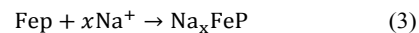
To understand the charge storage and transport mechanism of the CNT@FeP-C electrode, we conducted CV at various scan rates (Figure 4b). The CNT@FeP-C electrode demonstrates a typical conversion process, which is consistent with previous publications[19, 20]. The capacitive and diffusion contributions to electrochemical charge storage in the CNT@FeP-C electrode can be analyzed with varying scan rates according to the following equation[21]:

$$i = av^b\qquad(5)$$

where $a$ and $b$ are adjustable parameters, $i$ represents the current, and $v$ stands for the scan rate. The $b$-value can be determined from the slope by plotting log $i$ vs. log $v$. In particular, when $b$ = 0.5, the electrochemical process is limited by diffusion. Whereas $b$ = 1 suggests that the charge storage is dominated by a capacitive process. As shown in Figure 4b, the $b$ values were determined by the slopes from linear fitting of the curves of log($i$)
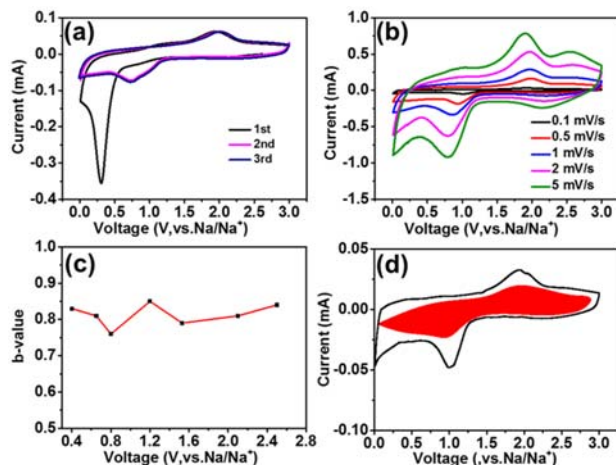
**Figure 4**. (a) Representative CV curves of the CNT@FeP-C nanocomposite at 0.1 mV s$^{-1}$ between 0.01 and 3.0 V, (b) CV curves of CNT@FeP-C at various sweep rates from 0.1 to 5 mV s$^{-1}$, (c) *b*-values and voltammetric response (0.5 mV$^{-1}$), and (d) Separation of capacitive (shaded region) and diffusion currents at a sweep rate of 0.5 mV s$^{-1}$.

vs. log($v$) in the cathodic process. The *b*-value was analyzed to be 0.76 at the cathodic peak (Fig 4c), which implied that the charge storage is mixed controlled. At potentials higher or lower than the peak potential, the *b*-value is in the range of 0.8~0.9, indicating that the capacitive process becomes dominant which is associated with the high rate performance of the electrode. Furthermore, to estimate the contribution from pseudocapacitive process at a small scan rate, we can distinguish it from the total current from the following formula:

$$\mathbf{i(V) = k_1 v + k_2 v^{1/2}} \tag{6}$$

$k_1 v$ and $k_2 v^{1/2}$ represent capacitive and diffusion-controlled contribution[22], respectively. By determining $k_1$ and $k_2$, it is possible to calculate the contributions from diffusion-controlled reaction and capacitor-like processes. The capacitive-controlled contribution (shaded region) at a scan rate of 0.5 mV s$^{-1}$ is shown in Figure 4d, which clearly indicates that the diffusion-controlled alloying/dealloying processes mainly occurs near the peaks and the capacitive contribution is about 52.7%.

In summary, we demonstrate a nanocomposite electrode composed of carbon coated mondispersed FeP nanoparticles anchored on a CNT network. The CNT network has the benefit of not only confining the active nanoparticle within flexible conductive hosts but also enhancing the conductivity to facilitate both electron and ion transport. Accordingly, the as-synthesized CNT@FeP-C electrode demonstrates excellent electrochemical performance in terms of long-term cycling (without obvious capacity decay after 1200 cycles) and superior rate capability (272 mAh g$^{-1}$ at a current density of 8 A g$^{-1}$). It is anticipated that the strategy shown in this work could be applied in designing other conversion-type electrode materials for high performance energy storage systems.

## Notes and references

1. J. W. Choi and D. Aurbach, *Nat Rev Mater*, 2016, **1**, 16013.
2. S. Kalluri, M. Yoon, M. Jo, H. K. Liu, S. X. Dou, J. Cho and Z. Guo, *Adv. Mater.*, 2017, **29**, 1605807.
3. N. Kim, S. Chae, J. Ma, M. Ko and J. Cho, *Nat. Comm.*, 2017, **8**, 812.
4. J. Liu, B. Ludwig, Y. Liu, Z. Zheng, F. Wang, M. Tang, J. Wang, J. Wang, H. Pan and Y. Wang, *Adv Mater Technol-Us*, 2017, **2**, 1700106.
5. J. Liu, J. G. Zhang, Z. G. Yang, J. P. Lemmon, C. Imhoff, G. L. Graff, L. Y. Li, J. Z. Hu, C. M. Wang, J. Xiao, G. Xia, V. V. Viswanathan, S. Baskaran, V. Sprenkle, X. L. Li, Y. Y. Shao and B. Schwenzer, *Adv Funct Mater*, 2013, **23**, 929-946.
6. J.-Z. Guo, P.-F. Wang, X.-L. Wu, X.-H. Zhang, Q. Yan, H. Chen, J.-P. Zhang and Y.-G. Guo, *Adv. Mater.*, 2017, **29**, 1701968.
7. J. L. Liu, Z. Chen, S. Chen, B. W. Zhang, J. Wang, H. H. Wang, B. B. Tian, M. H. Chen, X. F. Fan, Y. Z. Huang, T. C. Sum, J. Y. Lin and Z. X. Shen, *Acs Nano*, 2017, **11**, 6911-6920.
8. Q. M. Tang, Y. H. Cui, J. W. Wu, D. Y. Qu, A. P. Baker, Y. H. Ma, X. Song and Y. C. Liu, *Nano Energy*, 2017, **41**, 377-386.
9. Q. Wang, W. Zhang, C. Guo, Y. Liu, C. Wang and Z. Guo, *Adv Funct Mater*, 2017, **27**, 1703390.
10. Y. T. Wu, P. Nie, J. Wang, H. Dou and X. G. Zhang, *Acs Appl Mater Inter*, 2017, **9**, 39610-39617.
11. F. Han, C. Z. Zhang, J. X. Yang, G. Z. Ma, K. J. He and X. K. Li, *J Mater Chem A*, 2016, **4**, 12781-12789.
12. Z. Q. Li, L. Y. Zhang, X. L. Ge, C. X. Li, S. H. Dong, C. X. Wang and L. W. Yin, *Nano Energy*, 2017, **32**, 494-502.
13. X. J. Wang, K. Chen, G. Wang, X. J. Liu and H. Wang, *Acs Nano*, 2017, **11**, 11602-11616.
14. P. Scherrer, *Göttinger Nachrichten Math. Phys.*, 1918, **2**, 98-100.
15. Y. E. Zhu, L. P. Yang, J. Sheng, Y. N. Chen, H. C. Gu, J. P. Wei and Z. Zhou, *Adv Energy Mater*, 2017, **7,**1701222.
16. N. Takami, A. Satoh, M. Hara and I. Ohsaki, *J Electrochem Soc*, 1995, **142**, 371-379.
17. K. Zhang, M. Park, J. Zhang, G.-H. Lee, J. Shin and Y.-M. Kang, *Nano Res*, 2017, **10**, 4337-4350.
18. J. Zhang, K. Zhang, J. Yang, G. H. Lee, J. Shin, V. Wing-hei Lau and Y. M. Kang, *Adv Energy Mater*, 2018, **8,**1800283.
19. Y. Von Lim, S. Huang, Y. Zhang, D. Kong, Y. Wang, L. Guo, J. Zhang, Y. Shi, T. P. Chen, L. K. Ang and H. Y. Yang, *Energy Storage Materials*, 2018, **15**, 98-107.
20. Z. Huang, H. Hou, C. Wang, S. Li, Y. Zhang and X. Ji, *Chem. Mater.*, 2017, **29**, 7313-7322.
21. H. Lindstrom, S. Sodergren, A. Solbrand, H. Rensmo, J. Hjelm, A. Hagfeldt and S. E. Lindquist, *J Phys Chem B*, 1997, **101**, 7717-7722.
22. J. Wang, J. Polleux, J. Lim and B. Dunn, *J Phys Chem C*, 2007, **111**, 14925-14931.